ISSN 1674-1056
http://cpb.iphy.ac.cn
http://iopscience.iop.org/cpb
中国物理 B
Chinese Physics
中国物理 Chinese Physics B

High performance lateral Schottky diodes based on quasi-degenerated Ga_2O_3

Yang Xu(徐阳), Xuanhu Chen(陈选虎), Liang Cheng(程亮), Fang-Fang Ren(任芳芳), Jianjun Zhou(周建军), Song Bai(柏松), Hai Lu(陆海), Shulin Gu(顾书林), Rong Zhang(张荣), Youdou Zheng(郑有炓), Jiandong Ye(叶建东)

Citation: Chin. Phys. B . 2019, 28(3): 038503. **doi:** 10.1088/1674-1056/28/3/038503
Journal homepage: http://cpb.iphy.ac.cn; http://iopscience.iop.org/cpb

What follows is a list of articles you may be interested in

Structure-dependent behaviors of diode-triggered silicon controlled rectifier under electrostatic discharge stress

Li-Zhong Zhang(张立忠), Yuan Wang(王源), Yan-Dong He(何燕冬)
Chin. Phys. B . 2016, 25(12): 128501. **doi:** 10.1088/1674-1056/25/12/128501

Numerical and experimental study of the mesa configuration in high-voltage 4H-SiC PiN rectifiers

Xiao-Chuan Deng(邓小川), Xi-Xi Chen(陈茜茜), Cheng-Zhan Li(李诚瞻), Hua-Jun Shen(申华军), Jin-Ping Zhang(张金平)
Chin. Phys. B . 2016, 25(8): 087201. **doi:** 10.1088/1674-1056/25/8/087201

Thermoelectric properties of $Sr_{0.61}Ba_{0.39}Nb_2O_{6-\delta}$ ceramics in different oxygen-reduction conditions

Li Yi, Liu Jian, Wang Chun-Lei, Su Wen-Bin, Zhu Yuan-Hu, Li Ji-Chao, Mei Liang-Mo
Chin. Phys. B . 2015, 24(4): 047201. **doi:** 10.1088/1674-1056/24/4/047201

Electrical and dielectric properties of Al/p-Si and Al/perylene/p-Si type diodes in a wide frequency range

Ahmet Kaya, Sedat Zeyrek, Sait Eren San, Şmsettin Altindal
Chin. Phys. B . 2014, 23(1): 018506. **doi:** 10.1088/1674-1056/23/1/018506

Junction barrier Schottky rectifier with improved P-well region

Wang Ying, Li Ting, Cao Fei, Shao Lei, Chen Yu-Xian
Chin. Phys. B . 2012, 21(12): 128503. **doi:** 10.1088/1674-1056/21/12/128503

SPECIAL TOPIC — Photodetector: Materials, physics, and applications

High performance lateral Schottky diodes based on quasi-degenerated Ga_2O_3*

Yang Xu(徐阳)[1], Xuanhu Chen(陈选虎)[1], Liang Cheng(程亮)[1], Fang-Fang Ren(任芳芳)[1,2,3], Jianjun Zhou(周建军)[4], Song Bai(柏松)[4], Hai Lu(陆海)[1], Shulin Gu(顾书林)[1,2], Rong Zhang(张荣)[1,2], Youdou Zheng(郑有炓)[1,2], and Jiandong Ye(叶建东)[1,2,3,†]

[1] *School of Electronic Science and Engineering, Nanjing University, Nanjing* 210093, *China*
[2] *Collaborative Innovation Center of Solid-State Lighting and Energy-Saving Electronics, Nanjing University, Nanjing* 210093, *China*
[3] *Research Institute of Shenzhen, Nanjing University, Shenzhen* 518057, *China*
[4] *State Key Laboratory of Wide-Bandgap Semiconductor Power Electric Devices, The 55th Research Institute of China Electronics Technology Group Corporation, Nanjing* 210016, *China*

(Received 22 December 2018; revised manuscript received 14 January 2019; published online 28 January 2019)

Ni/β-Ga_2O_3 lateral Schottky barrier diodes (SBDs) were fabricated on a Sn-doped quasi-degenerate n^+-Ga_2O_3 ($\bar{2}01$) bulk substrate. The resultant diodes with an area of 7.85×10^{-5} cm^2 exhibited excellent rectifying characteristics with an ideality factor of 1.21, a forward current density (J) of 127.4 A/cm^2 at 1.4 V, a specific on-state resistance ($R_{on,sp}$) of 1.54 mΩ·cm^2, and an ultra-high on/off ratio of 2.1×10^{11} at ±1 V. Due to a small depletion region in the highly-doped substrate, a breakdown feature was observed at -23 V, which corresponded to a breakdown field of 2.1 MV/cm and a power figure-of-merit (V_B^2/R_{on}) of 3.4×10^5 W/cm^2. Forward current–voltage characteristics were described well by the thermionic emission theory while thermionic field emission and trap-assisted tunneling were the dominant transport mechanisms at low and high reverse biases, respectively, which was a result of the contribution of deep-level traps at the metal–semiconductor interface. The presence of interfacial traps also caused the difference in Schottky barrier heights of 1.31 eV and 1.64 eV respectively determined by current–voltage and capacitance–voltage characteristics. With reduced trapping effect and incorporation of drift layers, the β-Ga_2O_3 SBDs could further provide promising materials for delivering both high current output and high breakdown voltage.

Keywords: β-Ga_2O_3, Schottky diode, transport mechanism, quasi-degeneration, rectifier

PACS: 85.30.Hi, 72.20.Jv, 73.50.–h, 84.30.Jc **DOI:** 10.1088/1674-1056/28/3/038503

1. Introduction

Ultra-wide bandgap (UWBG) semiconductors are promising for the delivery of power electronic devices and deep-ultraviolet solar-blind photodetectors with high energy conversion efficiency which have versatile applications in electric power, industrial control, consumer electronics, automotive electronics industries, flame detection, missile guidance, biochemical detection, and space communication.[1–7] Among these UWBG materials, β-Ga_2O_3 is attracting significant interest owing to its highly projected Baliga's figure-of-merit (FOM) as a result of its wide-bandgap of 4.9 eV and large theoretical breakdown field of 8 MV/cm.[8–11] This is well in excess of the values of SiC and GaN, both of which are now established with commercial availability for high power devices. As β-Ga_2O_3 is one of the intrinsic solar-blind materials, state-of-the-art solar-blind photodetectors based on β-Ga_2O_3 Schottky diodes have been reported.[12–14] Compared to other UWBG materials including diamond and AlN, the availability of melt-growth methods to mass-produce single crystal β-Ga_2O_3 bulk substrates and the easy control of n-type doping provide important benefits towards low cost as well as the rapid development of epitaxial growth and device technologies. In recent years, rapid progress on the performance of field-effect transistors (FETs) and Schottky barrier diodes (SBDs) has been made.[15–22] With a low-doped drift layer grown by hydride vapor phase epitaxy (HVPE) and the integration of the field plates, vertical Schottky rectifiers with a breakdown voltage (V_B) of over 1 kV have been demonstrated.[15] Very recently, with the employment of a trench structure, SBDs without optimized field management techniques showed a 1230 V breakdown voltage and a decent on-resistance ($R_{on,sp}$ = 15 mΩ·cm^2).[16] There are also recent advances in the edge termination method that suppress the electric field and enhance the reverse breakdown voltages.[17–22]

*Project supported by the National Key R&D Program of China (Grant No. 2017YFB0403003), the National Natural Science Foundation of China (Grant Nos. 61774081, 61322403, and 91850112), the State Key R&D Project of Jiangsu, China (Grant No. BE2018115), Shenzhen Fundamental Research Project, China (Grant Nos. 201773239 and 201888588), State Key Laboratory of Wide-Bandgap Semiconductor Power Electric Devices, China (Grant No. 2017KF001), and the Fundamental Research Funds for the Central Universities, China (Grant Nos. 021014380093 and 021014380085).

†Corresponding author. E-mail: yejd@nju.edu.cn

© 2019 Chinese Physical Society and IOP Publishing Ltd

One of the merits of UWBG semiconductor-based SBDs is the improvement of their efficiency for applications in invertor circuits which need high current output. To date, most of the reported β-Ga_2O_3 SBDs are based on an unintentionally doped single crystal or thick epitaxial drift layer with a low carrier concentration. As a result, while the diode sustains extremely high critical electric fields, leading to large blocking voltages, high current output is limited. A tradeoff between high breakdown voltage and high forward current output remains an unsolved issue. Further improvement in the efficiency and functionality of invertors relies on high current output and speed, which can be realized by low on-state resistances using highly-doped wide-bandgap semiconductors. However, SBDs directly fabricated on highly-doped quasi-degenerated Ga_2O_3 materials are still challenging. Recently, only Oishi *et al.* reported on the fabrication of vertical SBDs directly on β-Ga_2O_3 single crystals with a high electron concentration of 3.9×10^{18} cm^{-3}.[23] Despite the fact that the diodes exhibit clear rectification characteristics with a current density of 96.8 A/cm^2 at the forward voltage of 1.6 V, there is still much room for improvement in the device performance, and also the conduction mechanism of devices on quasi-degenerated β-Ga_2O_3 is not fully understood. In this work, we demonstrated improved performance of SBDs in lateral configurations on a weakly-degenerated β-Ga_2O_3 ($\bar{2}$01) single crystal substrate with a high carrier concentration of 2×10^{18} cm^{-3}. The resultant lateral diodes showed excellent rectifying characteristics with an ultra-high rectification ratio of 2.1×10^{11} at ±1 V, an ideality factor of 1.21, a forward current density of 127.4 A/cm^2 at 1.4 V, and a specific on-state resistance $R_{on,sp}$ of 1.54 m$\Omega\cdot$cm^2. Furthermore, the associated transport mechanisms have been investigated in detail by means of current–voltage and capacitance–voltage characterizations.

2. Experimental details

All bulk substrates used in this work were square-shaped pieces cut from commercial 2-inch diameter, 500 μm-thick Sn-doped n-type ($\bar{2}$01) β-Ga_2O_3 wafers with a carrier concentration of 2×10^{18} cm^{-3} grown by the edge-defined film-fed growth (EFG) method. After chemically cleaning the β-Ga_2O_3 substrates with acetone, ethanol, and deionized water and subsequent lithography processing, the surface was selectively etched by an inductively coupled plasma (ICP) technique using a BCl_3 gas with a flow of 20 sccm for 80 s under a plasma/bias power of 400 W/30 W. The etch rate was measured at 15 nm/min using a profilometer. Then, Ti/Au metal stacks (100 nm/100 nm) were deposited by electron beam evaporation and annealed in nitrogen ambient at 650 °C for 60 s to ensure good Ohmic contacts. Subsequently, Ni/Au metal stacks (100 nm/100 nm) were selectively deposited as Schottky electrodes using an e-beam evaporator on the same side of the substrate by following a standard lithography procedure. Finally, through liftoff processes, circular Schottky contacts with diameters of 100 μm were formed. Figure 1(a) is a schematic of the planar β-Ga_2O_3 SBDs. The current–voltage (I–V) characteristics were measured using a Keithley source meter (model 2636A) and the capacitance–voltage (C–V) measurements were performed using a Keithley source meter model 4980A at the high frequency of 100 kHz. All measurements were performed at room temperature.

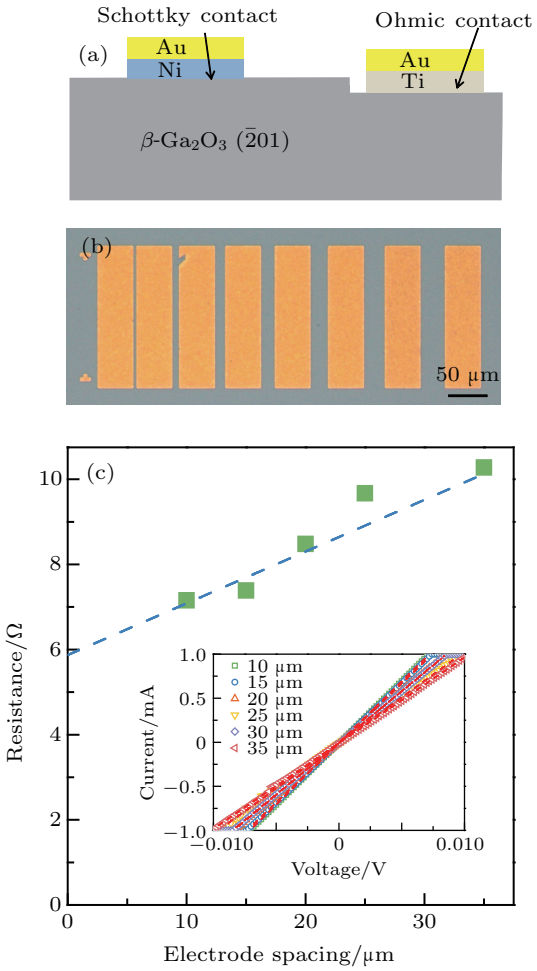


Fig. 1. (a) The geometry of the fabricated Schottky diodes. (b) Optical microscopy image of the TLM structures. (c) Total resistance between Ti/Au electrode spacing for $N_D = 2\times10^{18}$ cm^{-3}. The inset shows the I–V characteristics with different electrode spacings.

3. Results and discussion

Transmission line measurement (TLM) methods were employed to characterize the specific contact resistivity of the Ohmic electrodes. The electrodes for TLM tests are Ti/Au metal stacks (100 nm/100 nm) which were fabricated and annealed under the same conditions as the Ohmic contacts described above. The rapid thermal annealing process has been optimized with the condition of 650 °C for 60 s to reduce the contact resistance. It was found that surface pre-treatment by ICP processing increased the surface roughness and gener-

ated large-density donor-like surface defects, which is helpful for enhancing the Ohmic features and decreasing the contact resistance.[24] After ICP treatment, TLM structures with channel lengths varying from 10 μm to 35 μm were fabricated, as shown in Fig. 1(b). Figure 1(c) and its inset show the total resistance as a function of the channel length and the current–voltage behavior of the Ti/Au contacts with different channel lengths, respectively. Linear I–V features with different channel lengths are observed, indicating the nature of Ohmic contact to β-Ga_2O_3 by Ti/Au metal stacks. The total resistance between the electrodes is almost a linear function of the channel spacing. From Fig. 1(c), the sheet resistance (R_s) and specific contact resistance (R_c) were extracted to be 24.3 Ω/□ and 1.42×10^{-4} Ω·cm^2, respectively.

Figure 2 and its inset show the linear plot and semi-logarithmic plot of the J–V characteristics of the β-Ga_2O_3-based planar Schottky diodes with a diameter of 100 μm measured at room temperature (RT). In this work, the clamp current, which was set at 10 mA, was achieved at 1.4 V. Given the density of states (DOS) of the conduction band minimum (CBM) ($N_C = 3.8\times10^{18}$ cm^{-3}) for the β-Ga_2O_3 and a carrier concentration of 2×10^{18} cm^{-3}, the energy difference between the CBM and the Fermi level is about 23.7 meV, which is less than k_BT and indicative of weak degeneration of the β-Ga_2O_3 substrate. As a result, the large forward current density of 127.4 A/cm^2 was achieved at a rather small applied voltage of 1.4 V, which is much higher than other reported current densities. In particular, the main challenge of Schottky contact to a weak degenerated substrate is to maintain excellent rectifying features with low leakage currents due to a small depletion region and a high possibility of quantum tunneling transport across the barrier. A low leakage current density of 6×10^{-10} A/cm^2 at −1 V, reaching the measurement limitation of the source meter, was measured. It resulted in a high on/off current ratio up to 2.1×10^{11}, which is, to the best of our knowledge, one of the highest reported rectification ratios in β-Ga_2O_3-based Schottky devices. As shown in the inset of Fig. 2, the ideal thermionic emission (TE) theory could be used to fit well the relationship between the forward current density and voltage[23]

$$\begin{aligned} J &= J_0\exp\left(\frac{eV}{nk_BT}\right)\left[1-\exp\left(-\frac{eV}{nk_BT}\right)\right] \\ &= A^*T^2\exp\left(-\frac{e\varphi_B}{k_BT}\right)\exp\left(\frac{eV}{nk_BT}\right) \\ &\quad\times\left[1-\exp\left(-\frac{eV}{nk_BT}\right)\right], \end{aligned} \tag{1}$$

$$A^* = \frac{4\pi em^*k_B^2}{h^3}, \tag{2}$$

where e, n, k_B, h, T, J_0, A^*, m^*, and φ_B are the elementary charge, the ideality factor, the Boltzmann constant, the Plank constant, the temperature, the saturation current density, the effective Richardson constant, the electron effective mass, and the Schottky barrier height at equilibrium, respectively. The electron effective mass used of β-Ga_2O_3 is $m^* = 0.34m_0$, with m_0 being the free electron mass, and the value of A^* is 40.8 A/cm^2·K^2.[23] When $V > 3k_BT/e$ (∼ 0.078 V at room temperature), equation (1) can be simplified as

$$J = J_0\exp\left(\frac{eV}{nk_BT}\right). \tag{3}$$

Determined from Eq. (3), the ideality factor n is inversely proportional to the slope of the $\ln(J)$–V curve and fitting to the linear zone in the inset of Fig. 2 gives rise to the ideality factor $n = 1.21$. The causes of the n value being larger than 1 (unity) could be thermionic field emission tunneling, edge leakage, trap-assisted tunneling, and so forth, which tend to degrade the electron device performance characteristics. The saturation current density of 4.04×10^{-16} A/cm^2 and a Schottky barrier height of 1.31 eV can also be calculated, consistent with other reported values. Extracted by extrapolation from the linear zone in Fig. 2, the values of threshold voltage and on-resistance were obtained as 1.22 V and 1.54 mΩ·cm^2, respectively. Therefore, a low on-resistance and a small ideality factor prove the high conduction performance of the Schottky barrier diodes with Ni contacts upon forward bias. Reverse J–V characteristics of the Schottky barrier diode are shown in Fig. 3(a). The leakage current began to increase rapidly at −11 V and the results are repeatable. In the linear plot shown in Fig. 2, the current density increases sharply at −23 V with a length of depletion layer of 116 nm, a corresponding electric field of 2.10 MV/cm and a power figure-of-merit (V_B^2/R_{on}) of 3.4×10^5 W/cm^2.

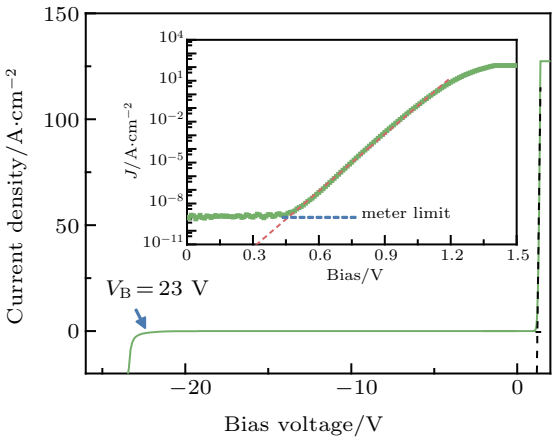


Fig. 2. Linear plot of J–V characteristics of the β-Ga_2O_3-based Schottky diodes with a diameter of 100 μm measured at room temperature. The inset is the semi-logarithmic plot of forward J–V.

To evaluate the plausibility of various conduction mechanisms responsible for the observed leakage current, analytical modeling of electrical transport properties in reverse bias

is necessary. For highly-doped weak-degenerated β-Ga_2O_3, the tunneling probability increases as electrons see a thinner barrier. It has been widely reported that the tunneling through thermionic field emission (TFE) becomes the favored transport phenomenon at reverse biases especially for high doping and intermediate temperatures.[25] Thermionic field emission takes place between field emission and thermionic emission.[25] When $k_BT \approx E_{00}$, the tunneling electrons have energy between the Fermi level of the metal and the conduction band edge of the dielectric. In this work, the current density at reverse bias below -4 V could be fitted well by the TFE model, which is given by[26]

$$J_{\rm TFE} = J_{00}\exp\left(\frac{eV}{\varepsilon'}\right), \tag{4}$$

$$\varepsilon' = \frac{E_{00}}{\left[\frac{E_{00}}{k_BT} - \tanh\left(\frac{E_{00}}{k_BT}\right)\right]}, \tag{5}$$

$$E_{00} = \frac{\hbar}{2}\sqrt{\frac{N_{\rm D}}{m^*\varepsilon_s\varepsilon_0}}, \tag{6}$$

where J_{00}, V, ε', E_{00}, $\hbar$, $N_{\rm D}$, m^*, and $\varepsilon_s\varepsilon_0$ are the saturation current density, the applied reverse bias, a temperature-dependent energy parameter that depends on the semiconductor doping, the Planck constant, the donor density, the electron effective mass, and the dielectric constant of the semiconductor, respectively. As shown in Fig. 3(a), the ln(J)–V plot can be fitted well by the TFE model at biases lower than 4 V and the slope of the linear variation of ln(J)–V allows the determination of the E_{00} parameters. The evaluated E_{00} value is 5.4 meV at room temperature, which is comparable to the thermal energy of $k_BT = 26$ meV at RT. Therefore, the observed exponential increase of the reverse leakage currents in the low reverse bias regime is governed by the tunneling transport mechanism through the TFE process as would be expected in most wide bandgap semiconductor-based Schottky diodes.

Furthermore, the evolution of reverse current at the high bias exhibits rather weak dependence on the applied voltages, which has also been observed in AlGaN-based Schottky diodes and is possibly contributed to by various field-enhanced tunneling mechanisms, such as the Pool–Frenkel (PF) emission, Fowler–Nordheim (FN) tunneling, or trap assisted tunneling (TAT) mechanisms.[25] When the reverse voltage is higher than -11 V, the length of the depletion layer is calculated to be larger than 80 nm and increases with the elevated bias. It was reported that the FN tunneling model becomes the dominant transport mechanism when the barrier is thin enough (<100 Å).[27] Thus, the FN mechanism can be excluded and the PF emission model was also found to fail to describe the leakage current at high reverse bias.[28–30] As a matter of fact, the current transport can be understood well by the TAT mechanism as expressed by[31,32]

$$J_{\rm TAT} = A_{\rm TAT}\exp\left(\frac{-8\pi\sqrt{2qm^*}}{3hE}\varphi_{\rm r}^{3/2}\right), \tag{7}$$

where $A_{\rm TAT}$, m^*, E, and $\varphi_{\rm r}$ are a constant, the electron effective mass, the electric field, and the energy of the electron traps with respect to the conduction band edge of the dielectric, respectively. It indicates that ln$J$ varies linearly with $\varphi_{\rm r}^{3/2}$, which can be observed in the J–V characteristics of the device as shown in Fig. 3(b). The plot of ln$J$ versus $1/E$ shows a good linear feature, and thus $\varphi_{\rm r}$ is extracted to be 1.05 V at high field values. The above analysis suggests that the interface traps are present at the metal–semiconductor interface, which reduce the Schottky barrier height or narrow the depletion region, leading to the carrier tunneling and large leakages. When the electric field approaches the breakdown point, the tunneling breakdown would possibly occur, leading to the remarkable increase in reverse leakage current, as shown in the part that does not follow the TAT model in Fig. 3(b).

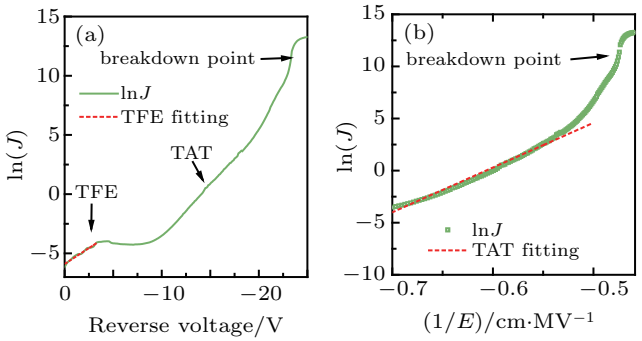


Fig. 3. (a) Linear fitting of ln(J)–V at low field by TFE and (b) linear fitting of ln(J)–$1/E$ at relatively high field by TAT.

Figure 4(a) shows the C–V and $1/C^2$–V plots of the Schottky barrier diodes measured at room temperature with 100 kHz sampling frequency. The capacitance decreases from 2.9×10^{-7} F/cm^2 to 1.44×10^{-7} F/cm^2 when the reverse bias is changed from 0 to -5 V due to the expanded depletion layer. The relationship between $1/C^2$ and the applied voltage can be expressed as[24]

$$\frac{1}{C^2} = \frac{2(\psi_{\rm bi} - V - k_BT/q)}{A^2q\varepsilon_s\varepsilon_0N_{\rm D}}, \tag{8}$$

where $\psi_{\rm bi}$, q, A, and $N_{\rm D}$ are the built-in voltage of the diode, the elementary charge, the contact area, and the electron concentration, respectively. Therefore, $\psi_{\rm bi}$ and $N_{\rm D}$ can be calculated from the intercept and the slope of a plot of $1/C^2$–V, respectively. The value of $N_{\rm D}$ extracted from the slope is about 1.96×10^{18} cm^{-3}, which is consistent with the Hall measurement results of the substrate given by Tamura Corporation, Japan. The Schottky barrier height is related to the built-in voltage and carrier concentration as given by[24]

$$\varphi_{\rm B} = \psi_{\rm bi} + \phi_{\rm n} + \frac{k_BT}{q}, \tag{9}$$

$$\phi_{\rm n} = E_{\rm C} - E_{\rm F} = k_{\rm B}T \ln \frac{N_{\rm C}}{N_{\rm D}}, \tag{10}$$

where $E_{\rm C}$, $E_{\rm F}$, and $N_{\rm C}$ are the conduction band minimum, the Fermi level, and the effective density of the states in the conduction band, respectively. The Schottky barrier height calculated from the C–V curve is 1.64 eV, which is higher than the one obtained from the forward J–V characteristics. The schematic energy band diagram of the Schottky contact between Ni and β-Ga_2O_3 is shown in Fig. 4(b). One cause of the difference in the barrier heights obtained from the I–V and C–V curves is the image force lowering effect, which normally affects the J–V characteristics with a negative effect on the barrier height while the C–V measurement at high frequency remains unaffected. However, the reduction in barrier height due to the image force lowering effect in this work is calculated to be only 0.125 eV, much smaller than the barrier difference of about 0.33 eV. Thus, image force lowering is not the main cause. It has been reported that the existence of interface traps could be the dominant cause of the difference.[33,34] As a result, the corresponding breakdown field is still lower than the expected theoretical value of 8 MV/cm. It is thus necessary to improve the interface quality of the metal–semiconductor contact to decrease the interface traps.

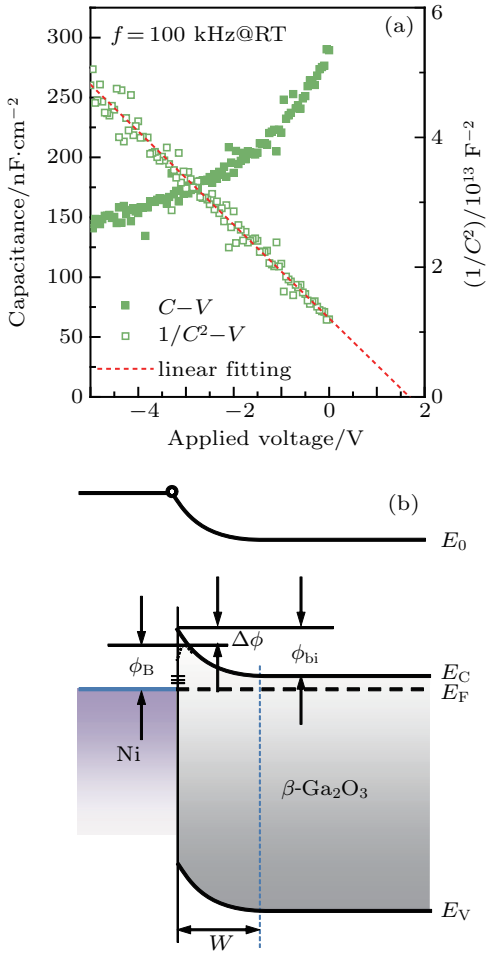


Fig. 4. (a) The C–V characteristics and $1/C^2$–V plots of the Schottky barrier diodes at room temperature with 100 kHz sampling frequency. (b) Schematic energy band diagrams of the Schottky contact between Ni and β-Ga_2O_3.

4. Conclusions

Planar geometry Schottky diodes were fabricated based on highly-doped β-Ga_2O_3 ($\bar{2}01$) substrates with an ultra-high rectification ratio of 2.1×10^{11}, a high current density of 127.4 A/cm^2 at 1.4 V, a low leakage of 6×10^{-10} A/cm^2, an ideality factor of 1.21, a low specific on-resistance of 1.54 mΩ·cm^2, and a power figure-of-merit ($V_{\rm B}^2/R_{\rm on}$) of 3.4×10^5 W/cm^2. The Schottky barrier height was calculated to be 1.31 eV and 1.64 eV from the I–V and C–V curves, respectively, and the difference mainly resulted from the existence of interface traps. Forward I–V characteristics were described well by the thermionic emission theory while thermionic field emission and trap-assisted tunneling are the dominant transport mechanisms at low and high reverse biases, respectively, which is a result of the contribution of deep-level traps at the metal–semiconductor interface. With reduced trapping effect, the performance of β-Ga_2O_3 SBDs could be further improved to deliver both high current output and high breakdown voltage.

References

[1] Yang C, Liang H, Zhang Z, Xia X, Tao P, Chen Y, Zhang H, Shen R, Luo Y and Du G 2018 *RSC Adv.* **8** 6341
[2] Jang S, Jung S, Kim J, Ren F, Pearton S J and Baik K H 2018 *ECS J. Solid State Sc* **7** Q3180
[3] Oshima T, Hashiguchi A, Moribayashi T, Koshi K, Sasaki K, Kuramata A, Ueda O, Oishi T and Kasu M 2017 *Jpn. J. Appl. Phys.* **56** 086501
[4] Oh S, Yang G and Kim J 2017 *ECS J. Solid State Sc* **6** Q3022
[5] Oishi T, Koga Y, Harada K and Kasu M 2015 *Appl. Phys. Express* **8** 031101
[6] Higashiwaki M, Konishi K, Sasaki K, Goto K, Nomura K, Thieu Q T, Togashi R, Murakami H, Kumagai Y and Monemar B 2016 *Appl. Phys. Lett.* **108** 133503
[7] Liu Z, Li P G, Zhi Y S, Wang X L, Chu X L and Tang W H 2019 *Chin. Phys. B* **28** 017105
[8] Hu Z, Zhou H, Feng Q, Zhang J, Zhang C, Dang K, Cai Y, Feng Z, Gao Y and Kang X 2018 *IEEE Electron Device Lett.* **39** 1564
[9] Yang J C, Ahn S, Ren F, Pearton S J, Jang S, Kim J and Kuramata A 2017 *Appl. Phys. Lett.* **110** 192101
[10] Farzana E, Zhang Z, Paul P K, Arehart A R and Ringel S A 2017 *Appl. Phys. Lett.* **110** 202102
[11] Ahn S, Ren F, Yuan L, Pearton S and Kuramata A 2017 *ECS J. Solid State Sc* **6** P68
[12] Oshima T, Okuno T, Arai N, Suzuki N, Hino H and Fujita S 2009 *Jpn. J. Appl. Phys.* **48** 011605
[13] Suzuki R, Nakagomi S, Kokubun Y, Arai N and Ohira S 2009 *Appl. Phys. Lett.* **94** 222102
[14] Pratiyush A S, Xia Z, Kumar S, Zhang Y, Joishi C, Muralidharan R, Rajan S and Nath D N 2018 *IEEE Photon. Technol. Lett.* **30** 2025
[15] Konishi K, Goto K, Murakami H, Kumagai Y, Kuramata A, Yamakoshi S and Higashiwaki M 2017 *Appl. Phys. Lett.* **110** 103506
[16] Li W, Hu Z, Nomoto K, Zhang Z, Hsu J Y, Thieu Q T, Sasaki K, Kuramata A, Jena D and Xing H G 2018 *Appl. Phys. Lett.* **113** 202101
[17] Yang J, Ahn S, Ren F, Pearton S, Jang S and Kuramata A 2017 *IEEE Electron Device Lett.* **38** 906
[18] Yang J C, Ren F, Tadjer M, Pearton S J and Kuramata A 2018 *AIP Adv.* **8** 055026
[19] Joishi C, Rafique S, Xia Z, Han L, Krishnamoorthy S, Zhang Y, Lodha S, Zhao H and Rajan S 2018 *Appl. Phys. Express* **11** 031101

[20] Sasaki K, Wakimoto D, Thieu Q T, Koishikawa Y, Kuramata A, Higashiwaki M and Yamakoshi S 2017 *IEEE Electron Device Lett.* **38** 783
[21] Kasu M, Oshima T, Hanada K, Moribayashi T, Hashiguchi A, Oishi T, Koshi K, Sasaki K, Kuramata A and Ueda O 2017 *Jpn. J. Appl. Phys.* **56** 091101
[22] Kasu M, Hanada K, Moribayashi T, Hashiguchi A, Oshima T, Oishi T, Koshi K, Sasaki K, Kuramata A and Ueda O 2016 *Jpn. J. Appl. Phys.* **55** 1202BB
[23] Oishi T, Harada K, Koga Y and Kasu M 2016 *Jpn. J. Appl. Phys.* **55** 030305
[24] He Q, Mu W, Dong H, Long S, Jia Z, Lv H, Liu Q, Tang M, Tao X and Liu M 2017 *Appl. Phys. Lett.* **110** 093503
[25] Rathkanthiwar S, Kalra A, Solanke S V, Mohta N, Muralidharan R, Raghavan S and Nath D N 2017 *J. Appl. Phys.* **121** 164502
[26] Hudait M and Krupanidhi S 2001 *Phys. B: Condens. Matter* **307** 125
[27] Chiu F C 2014 *Adv. Mater. Sci. Eng.* **7** 1
[28] Arslan E, Bütün S and Ozbay E 2009 *Appl. Phys. Lett.* **94** 142106
[29] Zhang H, Miller E J and Yu E T 2006 *J. Appl. Phys.* **99** 023703
[30] Sun X, Li D, Jiang H, Li Z, Song H, Chen Y and Miao G 2011 *Appl. Phys. Lett.* **98** 121117
[31] Sang L W, Ren B, Sumiya M, Liao M Y, Koide Y, Tanaka A, Cho Y J, Harada Y, Nabatame T, Sekiguchi T, Usami S, Honda Y and Amano H 2017 *Appl. Phys. Lett.* **111** 122102
[32] Sang L, Liao M, Koide Y and Sumiya M 2011 *Appl. Phys. Lett.* **98** 103502
[33] Freeouf J L, Jackson T N, Laux S E and Woodall J M 1982 *J. Vac. Sci. Technol.* **21** 570
[34] Ohdomari I and Tu K N 1980 *J. Appl. Phys.* **51** 3735